Versatile core-shell SiO_2@$SrTiO_3$:Eu^{c+}, Li^+ nanopowders as fluorescent label for the visualization of latent fingerprints and anti-counterfeiting applications

A. Sandhyarani, M.K. Kokila, G.P. Darshan, R.B. Basavaraj, B. Daruka Prasad, S.C. Sharma, T.K.S. Lakshmi, H. Nagabhushana

PII: S1385-8947(17)31041-0
DOI: http://dx.doi.org/10.1016/j.cej.2017.06.093
Reference: CEJ 17174

To appear in: *Chemical Engineering Journal*

Received Date: 5 April 2017
Revised Date: 11 June 2017
Accepted Date: 17 June 2017

Please cite this article as: A. Sandhyarani, M.K. Kokila, G.P. Darshan, R.B. Basavaraj, B. Daruka Prasad, S.C. Sharma, T.K.S. Lakshmi, H. Nagabhushana, Versatile core-shell SiO_2@$SrTiO_3$:Eu^{c+}, Li^+ nanopowders as fluorescent label for the visualization of latent fingerprints and anti-counterfeiting applications, *Chemical Engineering Journal* (2017), doi: http://dx.doi.org/10.1016/j.cej.2017.06.093

Versatile core-shell SiO_2@$SrTiO_3$:Eu^{3+}, Li^+ nanopowders as fluorescent label for the visualization of latent fingerprints and anti-counterfeiting applications

A. Sandhyarani [1, 2], M.K. Kokila[2], G. P. Darshan[3], R.B.Basavaraj[4], B. Daruka Prasad[5], S.C. Sharma[6, 7], T.K.S. Lakshmi[8], H. Nagabhushana[4, *]

[1]Department of Physics, Govt. Science College, Bengaluru-560 001, India

[2]Department of Physics, Bangalore University, Bangalore – 560 056, India

[3]Department of Physics, Acharya Institute of Graduate Studies, Bangalore 560 107, India

[4]Prof. C.N.R. Rao Centre for Advanced Materials, Tumkur University, Tumkur- 572 103, India

[5]Department of Physics, BMS Institute of Technology and Management, VTU-affiliated, Bangalore 560 064, India

[6]Advisor, Avinashilingam Institute for Home Science and Higher Education for Women University, Coimbatore 641043, India

[7]Department of Mechanical Engineering, Jain University, Advisor, Jain group of Institutions, Bangalore 560069, India

[8]Department of printing technology, Avinashilingam Institute for Home Science and Higher Education for Women University, Coimbatore 641043, India

Abstract

To overcome shortcomings encountered in enhancing the quality of latent finger prints (LFPs) by traditional powder dusting method, SiO_2@$SrTiO_3$:Eu^{3+} (1 mol %), Li (1 wt %) core–shell nanopowders (NPs) were prepared by using combustion process. LFPs were visualized by staining prepared samples on both porous and non-porous surfaces under the illumination of UV light of wavelength 254 nm. These LFPs reveals the detailed characteristic features such as lake, hook, island, bifurcation with high sensitivity, better selectivity and without background hindrance. SiO_2@$SrTiO_3$:EuLi NPs exhibited characteristic pure red emission peaks in the range of 530-760 nm which can be assigned to $^5D_0 \rightarrow {}^7F_J$ (J = 0, 1, 2 and 3) transitions. By altering the number of coating cycles dim white light fluorescent to warm white emitting phosphors could be obtained with the single crystal phase. The spectral intensity parameters and Eu-O ligand behaviors were estimated by means of Judd-Ofelt (J-O) theory. The prepared core-shell SiO_2@$SrTiO_3$:Eu^{3+}, Li NPs are explored as a fluorescent labeling agent for the visualization of latent fingerprints and anti-counterfeiting applications.

Keywords: Core shell; Latent fingerprints; Anti-counterfeiting; Photoluminescence, Judd-Ofelt analysis.

*** Corresponding author:** E-mail address: bhushanvlc@gmail.com (H. Nagabhushana).

1. Introduction

Nano research created many advantages in the field of surface-based science due to its quantum size effects and increased surface to volume ratio. This offers various possibilities in surface modified applications [1-3]. Latent fingerprint (LFP) is unique and utmost authoritative confirmation for the identification of persons due to its unique ridge patterns. The most frequently available LFPs at crime scenes are usually invisible or fewer visible to forensic scientists [4]. There are three different categories of characteristic LFP features were (i) normally identified namely pattern (level–I), (ii) minutia points (level-II) and (iii) sweat pores (level-III) [5-7]. Among them the second and third level features were highly useful for individual identification. Nevertheless, it was highly difficult to establish their ridge patterns, particularly the level-III features, which normally need high resolution techniques [8]. Additionally, the visualization of LFPs is frequently influenced by various parameters namely type of surface, environment and deposition age. Hence a high-resolution and simple procedure for visualization of LFPs was highly essential and has fascinated continuing interest for research community [9, 10].

Till date lot of techniques namely ninhydrin, iodine fuming, cyanoacrylate fuming and etc., were developed and adopted for visualization of LFPs. Conversely, some of these established approaches found numerous shortcomings namely less detection sensitivity, large background interference, complex operation and extremely harmfulness. Table 1 shows various reagents used for visualization of LFPs and their hazardous nature.

In order to tackle this issue, an eco-friendly method for developing LFPs with high sensitivity is the long-term goal for forensic experts. Further, already available commercial powders were highly agglomerated with micron sized and not uniform in shape. Such larger sized particles with uneven shapes have probability to diminish the affinity between the

powders and the LFP residuals. As a substitute to the conventional powders, fluorescent nanopowders (NPs) have received much devotion for the detection of LFPs owing to their smaller sized particles, huge surface area and large fluorescent intensity [11].

Recently, phosphors with uniform spherical core-shell morphology find numerous scientific and industrial applications due to their capability to fine tune the properties [12]. Two categories of templates were employed namely hard and soft for the fabrication of phosphors. Due to its tunable sizes, silica was regularly used in core-shell materials [13]. Nano/micron sized spherical SiO_2 core / shell can be prepared and widely used in core shell structured phosphors. The size of the phosphor particles was well controlled by means of silica core as well as number of coating layers.

Hence, for the first time we report the use of SiO_2@$SrTiO_3$:Eu^{3+} (1 mol %), Li (1 wt %) nanopowders (NPs) as a novel fluorescent labeling agent for visualization of LFPs on both porous and non-porous surfaces. Visualized LFPs reveal characteristic features such as lake, hook, island, bifurcation etc., with high sensitivity, selectivity and without background hindrance. The general idea of the present study was shown in Fig.1

2. Experimental

The micrometer sized uniform SiO_2 spheres were synthesized via well-known Stöber method [14]. In a typical synthesis tetraethyl orthosilicate (TEOS, 99 wt %) was added into 42.4 ml ethanol solution, 5.4 ml double distilled H_2O and 29.4 ml $NH_3 \cdot H_2O$ (25–28 wt %) to synthesize SiO_2 particles. The silica particles were centrifuged and washed several times with absolute ethanol and double distilled water. The obtained product was dried at 80 °C for 20 h. The core–shell structured $SrTiO_3$:Eu^{3+} (1mol %), Li (1 wt %) NP was synthesized by the combustion method. The stoichiometric quantities of Strontium nitrate: $Sr(NO)_3H_2O$ (Sigma Aldrich 99 %), Europium nitrate: $Eu(NO)_3$(Sigma Aldrich 99 %), Lithium nitrate: $LiNO_3$

(AR), Titanium (IV) isopropoxide: $Ti[OCH(CH_3)_2]_4$ (Sigma Aldrich 97 %), Citric acid: $[C_6H_8O_7]$ (Sigma Aldrich 99 %) and Polyethylene glycol: $C_{2n}H_{4n+2}O_{n+1}$ were dissolved in double distilled water. The SiO_2 particles obtained from Stöber route was added to the above solution and introduced into a pre-heated muffle furnace maintained at 500 ^oC. Due to the addition of citric acid into the reaction mixture, combustion took place instantaneously and forms NPs. Step by step reaction mechanism for the formation of $SrTiO_3:Eu^{3+}$: Li^+ NP on the surface of SiO_2 core shells was shown in Fig.2.

The phase purity of the obtained products were checked by Shimadzu-7000 powder X-ray diffractometer with Cu Kα radiation (λ=1.54Å). The microstructure and size of the samples were studied using Hitachi Table top scanning electron Microscope (SEM) and JEOL 2100 transmission electron microscopy (TEM) respectively. The excitation and emission spectra were recorded using Horiba Spectroflourimeter with 430 nm xenon excitation. The internal and external QEs based on the direct method and absorbance was measured by using the QE-2100 quantum efficiency measurement system from Otsuka Electronics. The fluorescence decay curves of Eu^{3+} were measured by a Horiba Fluorolog FL3-111 spectrometer with a scintillating xenon lamp.

Visualization of LFPs by staining $SiO_2@SrTiO_3:Eu^{3+}$ (1 mol %), Li^+ (1 wt %) NPs

Three main categories of porous and non-porous surfaces were identified for visualization of LFPs namely with a single background color (glass slide, ceramic floor tiles, paper cups, metallic surfaces, coins, goggles), with multiple background colors (marbles with composite patterns) and with strong background auto-fluorescence currency notes, debit cards and magazines covers). LFPs were collected from the same donor by washing hand with soap water and lightly wiped across the forehead. Then fingers were lightly pressed onto the various above mentioned surfaces. A dry prepared $SiO_2@SrTiO_3:Eu^{3+}$ (1 mol %), Li^+ (1

wt %) NP was cautiously deposited onto the different surfaces followed by a light brushing action to and fro to eliminate the surplus powder particles. A Nikon digital camera and 254 nm UV light source was used to photograph the images. The schematic representation to show visualization of LFPs on various surfaces including non-porous and porous materials using optimized $SiO_2@SrTiO_3:Eu^{3+}$ (1 mol %), Li^+ (1 wt %) NP was shown in Fig.3.

3. Results and Discussion

Fig.5. shows the PXRD patterns of SiO_2 and $SiO_2@SrTiO_3:Eu^{3+}$ (1 mol %), Li^+ (1 wt %) NPs. A characteristic broad peak at $2\theta = \sim 22.8^{\circ}$ clearly indicates amorphous SiO_2 (JCPDS card No. 29-0085) [15]. The diffraction peaks of $SiO_2@SrTiO_3:Eu^{3+}$ (1 mol %), Li^+ (1 wt %) NPs with single coating layer calcined at 500 ^{o}C for 3 h can be well indexed to cubic phase of $SrTiO_3$ (JCPDS card No. 35-0734) [16]. The single phase obtained in the spectra clearly evident that the Eu^{3+} ions were effectively replacing the Sr^{2+} or Ti^{4+} in the host $SrTiO_3$. Further, the strong and sharp diffraction peaks were observed with increase of the coating cycles and no additional phase was detected. These results evident further that the coated phosphor was highly crystalline on the surface of amorphous silica spheres and also the strong chemical stability towards temperature and moisture. Due to the extra coating layers of $SrTiO_3:Eu^{3+}$ (1 mol %), Li^+ (1wt %) on SiO_2 particles the average particles size of the $SiO_2@SrTiO_3:Eu^{3+}$ (1 mol %), Li^+ (1wt %) NPs were slightly larger than that of the pure silica particles.

Initially the citric acid forms chelates with Sr^{2+}, Eu^{3+}, Li+ and $(–O–Ti–O–)_n$ and subsequently crystalline grains of $SrTiO_3:Eu^{3+}$. Owing to uniform nucleation, the uneven crystalline grains will aggregate easily. To circumvent these difficulties, the core-shell silica spheres were added into the reaction mixture to endorse heterogeneous nucleation. The SiO_2 particles obtained from Stöber method contained huge amounts of -OH as well as Si–OH

groups on their surface and these groups play a vital role in bonding the Sr^{2+}, Eu^{3+} , Li^{+} and $(–O–Ti–O–)_n$ to form the $SrTiO_3:Eu^{3+}$, Li^{+} layers. When the Sr^{2+}, Eu^{3+}, Li^{+} and $(–O–Ti–O–)_n$ were adsorbed onto the surface of silica the $SrTiO_3:Eu^{3+}$, Li^{+} were probable to nucleate at the adsorbed locations [17]. This can clarify that why the crystallite size of $SrTiO_3:Eu^{3+}$, Li^{+} on the surface of silica particles is lesser than that of the $SrTiO_3:Eu^{3+}$, Li^{+} from combustion process which was comparable with the PXRD data.

Fig.5. shows the SEM and TEM images of SiO_2 particles and $SiO_2@SrTiO_3:Eu^{3+}$ (1 mol %), Li^{+} (1 wt %) NPs. The SiO_2 particles had a uniform spherical shape with smooth surface and average particles size was ~130 nm. The pure $SrTiO_3:Eu^{3+}$, Li particles were cubic shape. After coating with $SrTiO_3:Eu^{3+}$, Li the silica particles still retained the spherical shape, however even after four cycles of coating the surface become smooth. The average particle size was somewhat increase to 150 nm when silica nanoparticles were subjected to four cycles of coating. TEM images prove that the silica nanoparticles were covered with cubic shaped particles (Fig. 6(D)). Therefore, the coated particles had a core–shell structure. The respective differently coated nanoparticles fingerprints were observed in Fig. 7.

In order to fix the person involving in a crime, matching of minutiae points and pores were highly essential. Consequently, high-resolution LFPs with complete features were necessary for detection [18]. Figure 8 displays three levels of LFP ridge patterns comprising core (level 1), ridge ending (level 2), bifurcation (level 2), island/dot (level 2), scar (level 3), and pore (level 3). The magnified images from 1 to 3 level details in the FP established by means of dusting method validated its possibility for fingerprint detection.

To explain the background interference of the obtained sample on LFP detection, various porous materials were selected such as various types of paper, including train tickets, printing papers, magazine covers, and note papers (Fig. 9). LFP images on non-porous

materials such as stapler, spatula and punch pad as shown in Figure 10. The fingerprint images on the surface of paper cup, goggle and highlighter pen were also detected and shown in Fig. 11 and Fig. 12 respectively. To validate the usage of the fluorescent samples for the LFPs detection in forensic sciences, we conducted a series of experiments after the FPs had been aged for several periods of time. The detection sensitivity diminishes slowly with extended aging of the FPs, owing to the steady evaporation of the LFP. Conversely, the LFPs aged for up to 4 months could quiet are established a clear ridge a pattern, demonstrating that the sensitivity in the fluorescent phosphors based technique was high enough for aged LFPs development (Figure 13) and also in Table 2 [19 – 22].

To define the efficiency of red emitting phosphor for the development of LFPs on glass, conventionally used staining powders including Fe_2O_3, TiO_2 and commercial available fluorescent powder were used as a control (Figure 13). It was established that the magnetic as well as TiO_2 powders were not entirely develop the LFPs on glass. When the UV irradiation was incident to the LFPs stained by the customary fluorescent powders, the ridge patterns could not be clearly determined (Figure 14A - C). Nonetheless, when UV source was used to illuminate the FPs stained by fluorescent powder, the minutiae ridges of the FPs were clearly shown with sharp edges (Figure 14: A-1, A-2), displaying that the present powder can be used as an effective powder for the development of LFPs due to their enhanced strong red emission.

It was further evaluated the applicability of fluorescence based phosphor for detection of LFPs in genuine samples. Figure 15 (A, B) shows the LFPs detection on a piece of currency paper printed in blue ink. Although the blue ink might certainly interfere with the detection of LFPs, the high resolution and high contrast of the ridge particulars could still be clearly recognized. The same results could also be seen on credit card and coin

(Figure 15 C-F). The results confirmed that fluorescence based assay can be useful to a diversity of surfaces with complex backgrounds and will have an extensive usage in Forensic sciences.

For the past few decades, anti-counterfeiting has gained considerable attention due to extensive forgeries in variety of documents such as security of currency, tickets, certificates, cheque, trademarks, invoices etc. Fluorescent phosphors based anti-counterfeiting methods have significant consideration among all the existing methods and have developed necessary in this field by virtue of their great concealment properties. Here, SiO_2@$SrTiO_3$:Eu^{3+} (1 mol %), Li (1 wt %) NPs were integrated into a transparent PVA gold media to achieve UV exposed photo-luminescent anti-counterfeiting ink which exhibit a red color under ultraviolet light irradiation. This type of ink was appropriate for many printing modes namely dip pen writing, screen printing, gravure printing/letterpress printing, etc. Fig. 16 shows the digital photographs of the dip pen writing under natural as well as UV light irradiation. These pictures were fairly sharp and clear under 254 nm UV source, however, the images taken under white light was not clear under visible light (Figure 16: A1- D1). To authenticate the long-standing durability, we stored the writable images in a closed environment under bacterial atmosphere for 2 months. It was evident from Figure 16: A2- D2, the fluorescent properties of sample can retain for more than 2 months without substantial variations. Experimental data discussed were clearly evident for anti-counterfeit applications of prepared samples.

The PL excitation and emission spectra of $SrTiO_3$:Eu^{3+} (1mol %), $SrTiO_3$:Eu^{3+} (1 mol %), Li^+ (1wt %) and SiO_2@$SrTiO_3$:Eu^{3+} (1 mol %), Li (1wt %) phosphors were studied under 395 nm excitation and shown in Figure 17 (a, b). The PLE spectra consist of broad charge transfer (CT) band at 240-355 nm was ascribed to $Eu^{3+} \rightarrow O^{2-}$. Further, the sharp peaks at ~361 nm, 381 nm and 393 nm were corresponds to the f-f transitions of $^7F_0 \rightarrow {}^5D_4$, $^7F_0 \rightarrow {}^5L_7$)

($^7F_0 \rightarrow {}^5L_6$), respectively [23]. Further, it was observed that the CT bands in SiO_2 coated phosphors were shifted towards higher wavelength when compared to without coated phosphor. In addition to this the intensity peaks for 395 nm enhances with the coating cycles. The higher wavelength shift was related with the electronic structure of $SrTiO_3:Eu^{3+}$ shells on SiO_2 core shells. The intense excitation peak at 393 nm was well matched with the output wavelength of NUV (350-400 nm) chip in pc-WLED [24]. Hence $SiO_2@SrTiO_3:Eu^{3+}$(1 mol %),Li (1wt %) phosphor could be highly useful for red emitting LED's. Further the increased wavelength affects the energy band gap to decrease, this indicates that the overall stability of the core-shell increased and the material becomes the red shift semiconducting type.

The emission spectra (Figure 17b) composed of intense peaks of Eu^{3+} ions at 591 nm ($^5D_0 \rightarrow {}^7F_1$), 612 nm ($^5D_0 \rightarrow {}^7F_2$), 646 nm ($^5D_0 \rightarrow {}^7F_3$), 696 nm ($^5D_0 \rightarrow {}^7F_4$). Among these transitions, the orange–red emission peak at 612 nm was electric dipole transition and 591 nm peaks correspond to magnetic dipole ($^5D_0 \rightarrow {}^7F_1$) which depends largely on the local symmetry of the Eu^{3+} ion [25]. It was evident that PL intensity was increasing almost one fold in Li doped and 2 folds in SiO_2 coated phosphors when compared to uncoated ones. The coating cycles play a vital role in enhancing the PL intensity of the phosphor (Figure 17 c, d). The PL intensity was increase with phosphor coating. The growth of the PL intensity was ascribed to the increase of the shell thickness on the SiO_2 cores which was due to large quantity of emitting ions (Eu^{3+}) per core-shell phosphors. As anticipated that external coating may be effective in order to increase the thermal stability of any phosphors. Hence to explain the essential mechanism, the coated and non-coated phosphors were calcined at 800 ^oC and shown in Figure 17 (b & c). It was evident that after calcination, the emission intensity found to be lower, but the rate of declining was different. The integrated emission intensity was ~ 94% for the phosphor coated four cycles on SiO_2 cores shells and 78 % for the non-coated phosphors. The effect of Li ions on PLE was checked under NUV excitation wavelength and

found that emission intensity of the SiO_2@$SrTiO_3$:Eu^{3+}(1 mol %),Li (1wt %)NPs was higher than that of SiO_2@$SrTiO_3$:Eu^{3+}(1 mol %). Here,Li ions can be act as charge compensator, leading to the improved luminescence of Eu^{3+} in $SrTiO_3$.Phosphors coated on core-shells have wide range of applications including solid state lighting, sensors, fuel cells, catalysts etc. Further, core-shell phosphors will reduce the cost and can be prepared in large quantity. Therefore applying numerous phosphor coatings to the silica core shells can engineered the numerous structures and can develop fascinating applications.

Judd–Ofelt (J-O) intensity parameters Ω_t (t= 2, 4, 6) were used to determine influence of the spectroscopic environment of the dopant ions and the site symmetry of dopant in$SrTiO_3$host [25]. From J-O intensity parameters, radiative properties namely radiative transition probability (A_T), radiative life time (τ_{rad}), branching ratio (β_R), asymmetric ratio (A_{21}) and stimulated emission cross-section (σ_e) of $Eu^{3+}$and Li ions in $SrTiO_3$:Eu^3 host were estimated. These parameters were estimated by the procedures explained elsewhere [26]. The measured branching ratio values for $SrTiO_3$:Eu^{3+}:Li nanophosphor was found to be 0. 99 ≥ 0.50 and was potential for stimulated emission, which can emit laser radiation more effectively and suitable for red emitting display devices. The calculated values of emission cross sections were estimated given in Table 3.

The CIE (Commission Internationale de I'Eclairage) chromaticity coordinates and CCT (correlate colour Temperature) [27] of $SrTiO_3$:Eu^{3+}, $SrTiO_3$:Eu^{3+}, Li, SiO_2@$SrTiO_3$:Eu^{3+}(1 mol %),Li (1wt %) phosphors were calculated using PLE spectra and obtained values were summarized in Table 4 and CIE and CCT diagrams are shown in Figure 17 (e, f). With increasing the $SrTiO_3$:Eu^{3+}, Li coating cycles on the SiO_2 particles, the CIE chromaticity coordinates (x, y) shifted from orange-red (0.488, 0.295) to deep red (0.653, 0.339) which was close to the standard of National Television Standards Committee (0.67, 0.33). Based on the values of CCT, the color quality of light was determined and the

lesser the CCT values were necessary for efficient display devices [28]. The CCT of the core shell phosphors were estimated using McCamy empirical formula, CCT = $-449n^3 + 3525n^2 - 6823n + 5520.33$ where $n = x-x_e/y-y_e$; inverse slope of the line and $x_e$and y_e values are 0.332 and 0.186. Among all the combinations, the CIE and CCT of SiO_2@$SrTiO_3$:Eu^{3+}(1 mol %),Li (1wt %)phosphors lies in x = 0.5491, y = 0.4150 with 3921 K indicates the phosphor lies in the light white fluorescent point in standard illuminants [29]. In addition, without addition of core-shells the phosphors shows cool white fluorescence. These results specify that by altering the number of coating cycle's it is able to tune white fluorescent to warm white emitting phosphors and it could be able to obtained in single crystal phase.

Figure 18 displays the decay profiles of un-coated $SrTiO_3$:Eu^{3+}, $SrTiO_3$:Eu^{3+}, Li and $SrTiO_3$: Eu^{3+}, Li coated SiO_2 phosphors upon excitation wavelength of 395 nm. As can be seen from figure, the decay profiles of SiO_2 coated phosphors have similar trend with the non-coated SiO_2 phosphors. This phenomena was further established that the structure remain same even after SiO_2 coating. However, the decay time was found to merely faster in SiO_2 coated phosphors than that of without coated. This mainly attributed to presence of deeper trap densities in SiO_2 coated phosphors related to uncoated ones [30]. Further, SiO_2 acts as a shielding layer that hinders the diffusion of oxygen ions into the phosphors thus decreasing thermal degradation and improving thermal stability.

To understand luminescence decay performance the decay data was fitted with different decay relations. It was establish that curves follow dual types of exponential decays for without and with SiO_2 coated phosphors respectively in the $SrTiO_3$ host (i) bi-exponential decay (ii) tri exponential decay.

$$I(t) = I_1 e^{-\frac{1}{\tau 1}} + I_2 e^{-\frac{1}{\tau 2}} \qquad \text{-------- (1)}$$

where I_1 and I_2 are intensities at different times and their corresponding lifetimes τ_1 and τ_2.

The average lifetime in case of tri-exponential decay can be estimated by using the following equation:

$$\tau_{avg} = \frac{I_1\tau_1^{\ 2} + I_2\tau_2^{\ 2}}{I_1\tau_1 + I_2\tau_2} \qquad \text{-------- (2)}$$

$$I(t) = I_1 e^{-\frac{1}{\tau_1}} + I_2 e^{-\frac{1}{\tau 2}} + I_3 e^{-\frac{1}{\tau 3}} \qquad \text{-------- (3)}$$

The average lifetime in case of tri-exponential decay can be estimated by using the following equation:

$$\tau_{avg} = \frac{I_1\tau_1^{\ 2} + I_2\tau_2^{\ 2} + I_3\tau_3^{\ 2}}{I_1\tau_1 + I_2\tau_2 + I_3\tau_3} \qquad \text{---------- (4)}$$

where I_1, I_2 and I_3 are the intensities oat different times and their corresponding lifetimes τ_1, τ_2 and τ_3 respectively.

Quantum efficiency (QE) of the optimized samples was estimated using the relation as reported elsewhere [31 -33]:

$$QE = \frac{Number\ of\ Photons\ emitted}{Number\ of\ Photons\ absorbed} = \frac{E_c - E_a}{L_a - L_c} \qquad \text{……(5)}$$

where, E_C ; the integrated luminescence of the phosphor caused by direct excitation, E_a ; the integrated luminescence from the empty integrating sphere (blank, without sample), L_a; the integrated excitation profile from the empty integrating sphere, L_c; the integrated excitation profile when the sample is directly excited by the incident beam. In the present case, the estimated value of QE was found to be ~ 91.23 % for SiO_2@$SrTiO_3$:Eu^{3+} (1 mol %), Li^+ (1 wt %) NPs, suggest the high QE of the prepared sample.

Conclusions

The SiO_2@$SrTiO_3$:Eu^{3+} (1 mol %), Li (1 wt %) phosphors with a core–shell structures have been effectively fabricated by a solution based combustion route. The obtained core–shell particles display a uniform spherical morphology with narrow size distribution as well as good dispersion. From SEM and TEM analysis the $SrTiO_3$:Eu^{3+}, Li^+ NPs were successfully coated on SiO_2 core shell particles, which can be further confirmed by PXRD. The CIE chromaticity coordinates of SiO_2@ $SrTiO_3$:Eu^{3+} (1 mol %): Li^+ (1 wt %) NPs change from orange-red to the deep red with increase up to 4 coating cycles. The PL intensity can be tuned by controlling the coating number and a 2 fold enhancement in PL intensity was observed after 4 cycles of coating. The integrated emission intensity was ~ 94% for the phosphor coated four cycles on SiO_2 cores shells and 78 % for the non-coated phosphors. The core–shell phosphors achieved in combustion method was effective and can be preparing several other rare earth doped phosphors with cost effective and uniform morphology. Core–shell phosphors obtained have several potential applications including displays, fingerprint detection anti-counterfeiting etc. SiO_2 coated phosphors acts as a shielding layer that hinders the diffusion of oxygen ions into the phosphors thus decreasing thermal degradation and improving thermal stability. By altering the number of coating cycles lite white fluorescent to warm white emitting phosphors could be obtained in single phase.

Acknowledgement

The author Dr. H Nagabhushana thanks to DST Nano Mission (Project No. SR/NM/NS- 48/2010) New Delhi for the sanction of this Project.

References

[1] M. G. Mendez Medrano, E. Kowalska, A. Lehoux, A. Herissan, B. Ohtani, Bahena, D. C. Colbeau-Justin, J. L. Rodriguez Lopez, Remita, H., Surface Modification of TiO_2 with Ag Nanoparticles and CuO Nanoclusters for Application in Photocatalysis. J. Phys. Chem. C**.** 120(2016) 5143–5154.

[2] W. D. Robert, N. M. Max, M.L. Charles, Plateau–Rayleigh Crystal Growth of Nanowire Heterostructures: Strain-Modified Surface Chemistry and Morphological Control in One, Two, and Three Dimensions. Nano Lett.16 (2016) 2830-2836.

[3] J. Piella, N. G. Bastus, V. Puntes, Size-Controlled Synthesis of Sub-10-nanometer Citrate-Stabilized Gold Nanoparticles and Related Optical Properties. Chem. Mater. 28 (2016) 1066-1075.

[4] B. Li, X. Zhang, L. Zhang, T. Wang, L. Li, C. Wang, Z. Su, NIR-responsive $NaYF_4$: Yb, Er, Gd fluorescent upconversion nanorods for the highly sensitive detection of blood fingerprints. Dyes Pigm.134 (2016) 178-185.

[5] X. Tang, L. Huang, W. Zhang, H. Zhong, Chemical imaging of latent fingerprints by mass spectrometry based on laser activated electron tunneling. Anal. Chem. 87 (2015) 2693–2701.

[6] A.K. Jain, Y. Chen, M. Demirkus, Pores and Ridges: High-Resolution Fingerprint Matching Using Level 3 Features. IEEE Trans. Pattern Anal. Mach. Intell.29 (2007) 15-27.

[7] R. Cappelli, M. Ferrara, A fingerprint retrieval system based on level-1 and level-2 features. Expert Syst. Appl.39 (2012) 10465–10478.

[8] M.J. Choi, A.M. McDonagh, P. Maynard, C. Roux, Metal-containing nanoparticles and nano-structured particles in fingermark detection. Forensic Sci. Int.179 (2008) 87–97.

[9] C. Xu, R. Zhou, W. He, L. Wu, P. Wu, X. Hou, Fast imaging of eccrine latent fingerprints with nontoxic Mn-doped ZnS QDs. Anal. Chem.86 (2014) 3279 – 3283.

[10] A. Becue, S. Moret, C. Champod, P. Margot, Fast imaging of eccrine latent fingerprints with nontoxic Mn-doped ZnS QDs. Use of stains to detect fingermarks, Biotechnic & Histochemistry.86 (2011) 140-160.

[11] Y. Ma, H. Li, S. Peng, L. Wang, Highly selective and sensitive fluorescent paper sensor for nitroaromatic explosive detection. Anal. Chem.84 (2012) 8415−8421.

[12] W. Suna, Y. Gua, Q. Zhanga, Y. Li, H. Wanga, $CaTiO_3$: Eu^{3+} layers coated SiO_2 particles: core-shell structured red phosphors for near-uv white LEDs. J. Alloys Compd.493 (2010) 561–564.

[13] J. Dai, M. Lv, G. Li, X. Li, Synthesis and luminescence properties of highly uniform SiO_2@ $LaPO_4$: Eu^{3+} core–shell phosphors. Materials & Design.83 (2015) 795–800.

[14] N. Bayal, P. Jeevanandam, Synthesis of SiO_2@NiO magnetic core–shell nanoparticles and their use as adsorbents for the removal of methylene blue. J Nanopart Res.15 (2013) 2066.

[15] M. Yu, H Wang, C.K. Lin, G.Z. Li, J. Lin, Sol–gel synthesis and photoluminescence properties of spherical SiO_2@ $LaPO_4$: Ce^{3+}/Tb^{3+} particles with a core–shell structure. Nanotechnology17 (2006) 3245–3252.

[16] N. P. Bhagya, P. A. Prashantha, R. S. Raveendra, S. Sathyanarayani, S. Ananda, B. M. Nagabhushana, H. Nagabhushana, Adsorption of hazardous cationic dye onto the combustion derived $SrTiO_3$ nanoparticles: Kinetic and isotherm studies. J. Asian Ceram. Soc.4 (2015) 68-74.

[17] Z.Q. Zhang, C. Chen, C. Ma, M. Li, H. Chen, Z.G. Shang, MnO_2 Density-Dependent Supercapacitive Characteristics of SiO_2/MnO_2 Core-shell Nanostructure. Int. J. Electrochem. Sci.11 (2016) 6138 – 6148.

[18] B.Errington, G.Lawson, S.W.Lewis, G.D.Smith, Micronised Egyptian blue pigment: A novel near-infrared luminescent fingerprint dusting powder. Dyes Pigm.132 (2016) 310-315.

[19] Mi Jung Choi, Tanya Smoother, Aiden A. Martin, Andrew M. McDonagh, Philip J. Maynard, Chris Lennard, Claude Roux, Fluorescent TiO2 powders prepared using a new perylene diimide dye: applications in latent fingermark detection, Forensic Sci. Int., 173 (2007) 154-160.

[20] L. Liu, Z. Zhang, L. Zhang, Y. Zhai, The effectiveness of strong afterglow phosphor powder in the detection of fingermarks, Forensic Sci. Int. 183 (2009) 45-49.

[21] M. Wang, Y. Zhu, C. Mao, Synthesis of NIR-Responsive NaYF4Yb,Er Upconversion fluorescent nanoparticles using an optimized solvothermal method and their applications in enhanced development of latent fingerprints on various smooth substrates, Langmuir, 31 (2015) 7084-7090.

[22] R. B. Basavaraj, H. Nagabhushana, G. P. Darshan, B. Daruka Prasad, S. C. Sharma, K. N. Venkatachalaiah, Ultrasound assisted rare earth doped Wollastonite nanopowders: Labeling agent for imaging eccrine latent fingerprints and cheiloscopy applications, J. Industrial Engg. Chem., 51 (2017) 90-105.

[23] D.Prakashbabu, H.B.Ramalingam, R.Hari Krishna, B.M.Nagabhushana, R.Chandramohan, C.Shivakumara, J.Thirumalai, Tiju Thomas, Charge compensation assisted enhancement of photoluminescence in combustion derived Li^{+} co-doped cubic ZrO_2: Eu^{3+} nanophosphors. Phys. Chem. Chem. Phys.18 (2016) 29447-29457.

[24] 20. V.Sharma, A.Das, V.Kumar, O.M.Ntwaeaborwa, H.C.Swart, Potential of $Sr_4Al_{14}O_{25}$: Eu^{2+}, Dy^{3+} inorganic oxide-based nanophosphor in Latent fingermark detection. J Mater Sci.49 (2014) 2225-2234.

[25] 21. P.K.Jisha, Ramachandra Naik, S.C.Prashantha, H.Nagabhushana, S.C.Sharma, H.P.Nagaswarupa, K.S.Anantharaju, B. Daruka Prasad, H.BPremkumar, Potential of $Sr_4Al_{14}O_{25}$: Eu^{2+}, Dy^{3+} inorganic oxide-based nanophosphor in Latent fingermark detection. J. Lumin. 163 (2015) 47-54.

[26] 22. K. Mondal, P. Kumari, J. Manam, Influence of doping and annealing temperature on the structural and optical properties of Mg_2SiO_4: Eu^{3+} synthesized by combustion method. Curr. Appl Phys. 16 (2016) 707-719.

[27] R.B.Basavaraj, H. Nagabhushana, B. Daruka Prasad, S.C.Sharma, S.C.Prashantha, B.M.Nagabhushana, A single host white light emitting Zn_2SiO_4: Re^{3+} (Eu, Dy, Sm) phosphor for LED applications. Optik126 (2015) 1745-1756.

[28] M. Venkataravanappa, H. Nagabhushana, B. Daruka Prasad, G.P. Darshan, R.B. Basavaraj, G.R. Vijayakumar, Dual color emitting Eu doped strontium

orthosilicate phosphors synthesized by bio-template assisted ultrasound for solid state lightning and display applications. Ultrason Sonochem.34 (2017) 803–820.

[29] Danny C. Rich, A review of solid-state lighting and its impact on the marketing and production of decorative coatings. J. Coat. Technol. Res.13 (2016) 1-9.

[30] Y. Zhu, M.Zheng, J.Zeng, Y.Xiao Y.Liu, Luminescence enhancing encapsulation for strontium aluminate phosphors with phosphate. Mater. Chem. Phys. 113 (2009) 721–726.

[31] K. N. Venkatachalaiah, H. Nagabhushana, G. P. Darshan, R. B. Basavaraj, B. Daruka Prasad, Sensor Actuators B 251 (2017) 310-325.

[32] M. Shivram, S.C. Prashantha, H. Nagabhushana, S.C. Sharma, K. Thyagarajan, R. Harikrishna, B.M. Nagabhushana, $CaTiO_3:Eu^{3+}$ red nanophosphor: Low temperature synthesis and photoluminescence properties, Spec. chim. Acta Part A: Mol. Biomol. Spec.120 (2014) 395–400.

[33] N. Dhananjaya, H. Nagabhushana, B.M. Nagabhushana, B. Rudraswamya, C. Shivakumara, R.P.S. Chakradhar, Effect of Li^+-ion on enhancement of photoluminescence in $Gd_2O_3:Eu^{3+}$ nanophosphors prepared by combustion technique, J. Alloys Compd.509 (2011) 2368–2374.

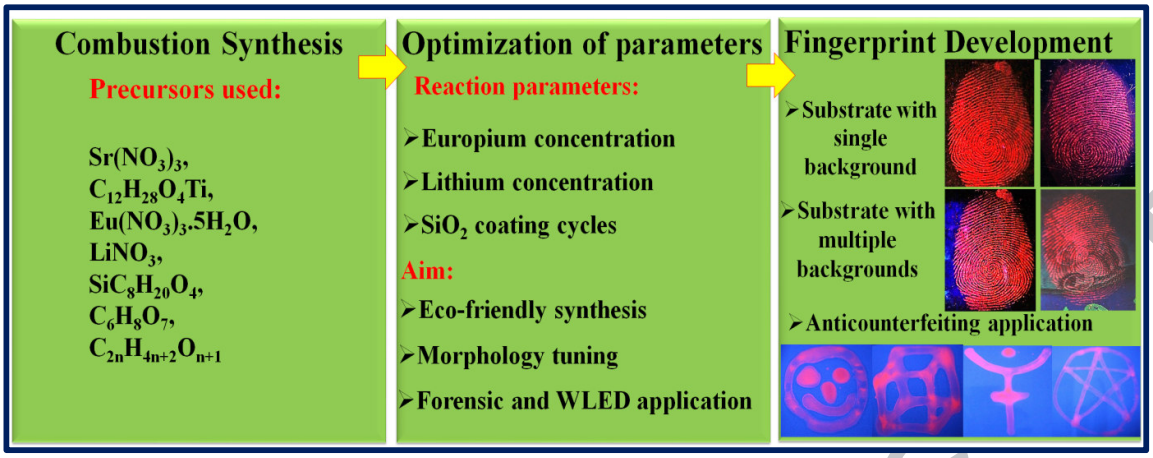

Fig.1. General idea of the present study.

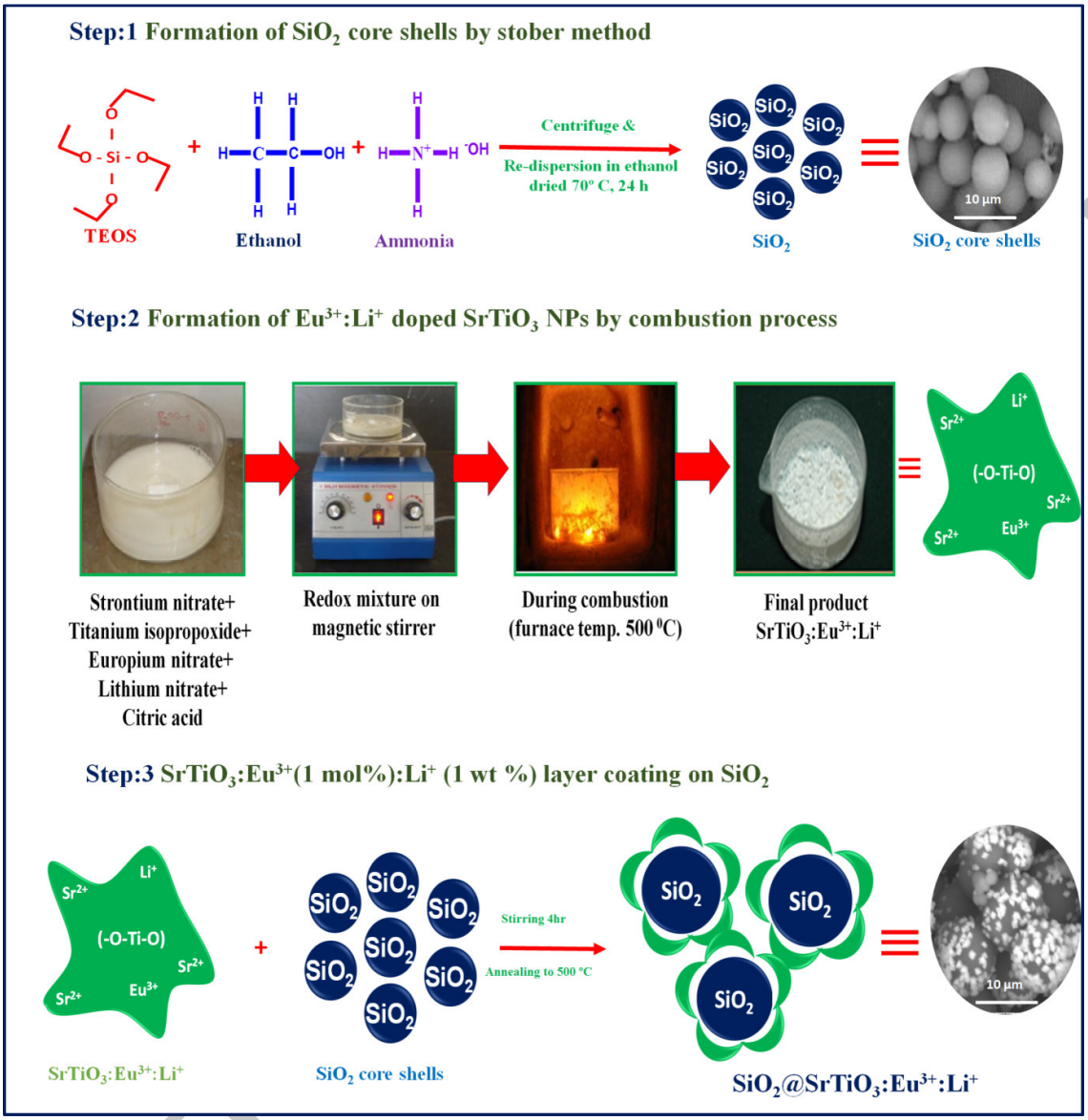

Fig.2.Step by step reaction mechanism for the formation of $SrTiO_3:Eu^{3+}$: Li^+ NP on the surface of SiO_2 core shells.

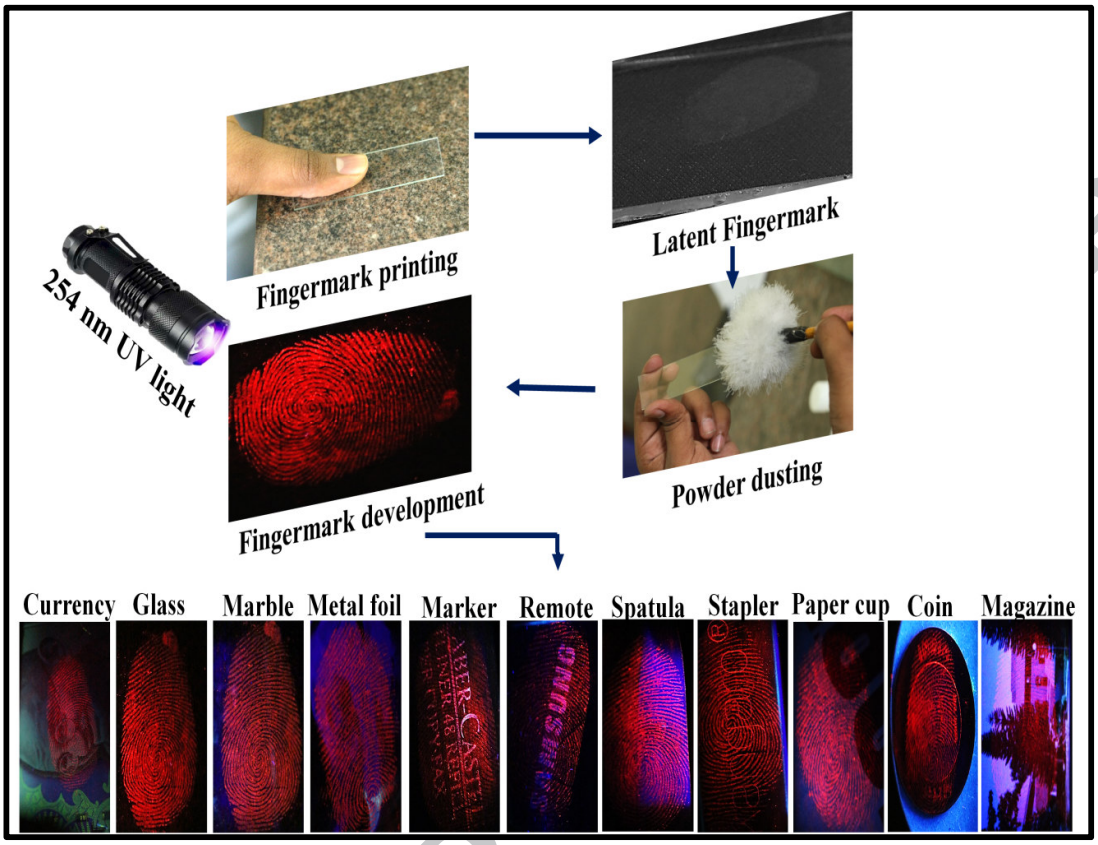

Fig.3. Pictorial representation of visualization of LFPs on various surfaces including non-porous and porous materials using optimized SiO_2@$SrTiO_3$:Eu^{3+} (1 mol %), Li^+ (1 wt %) NP.

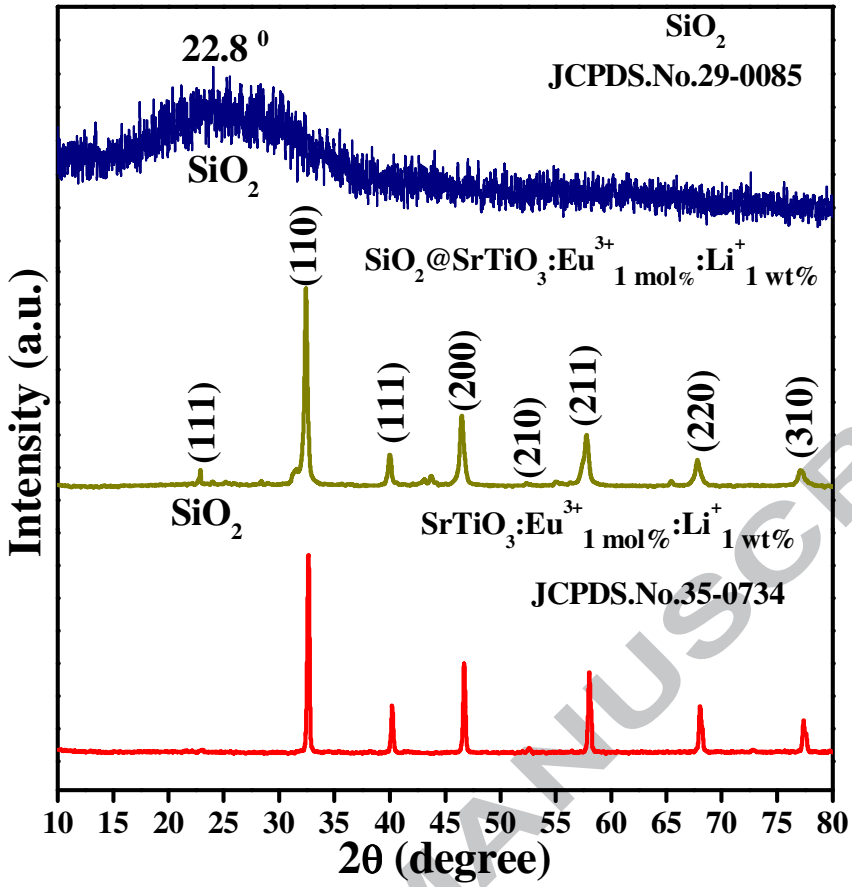

Fig.4. PXRD patterns of SiO_2, SiO_2@$SrTiO_3$:Eu^{3+}(1 mol %):Li^+ (1 wt %) and $SrTiO_3$:Eu^{3+} (1 mol %):Li^+ (1 wt %) NPs.

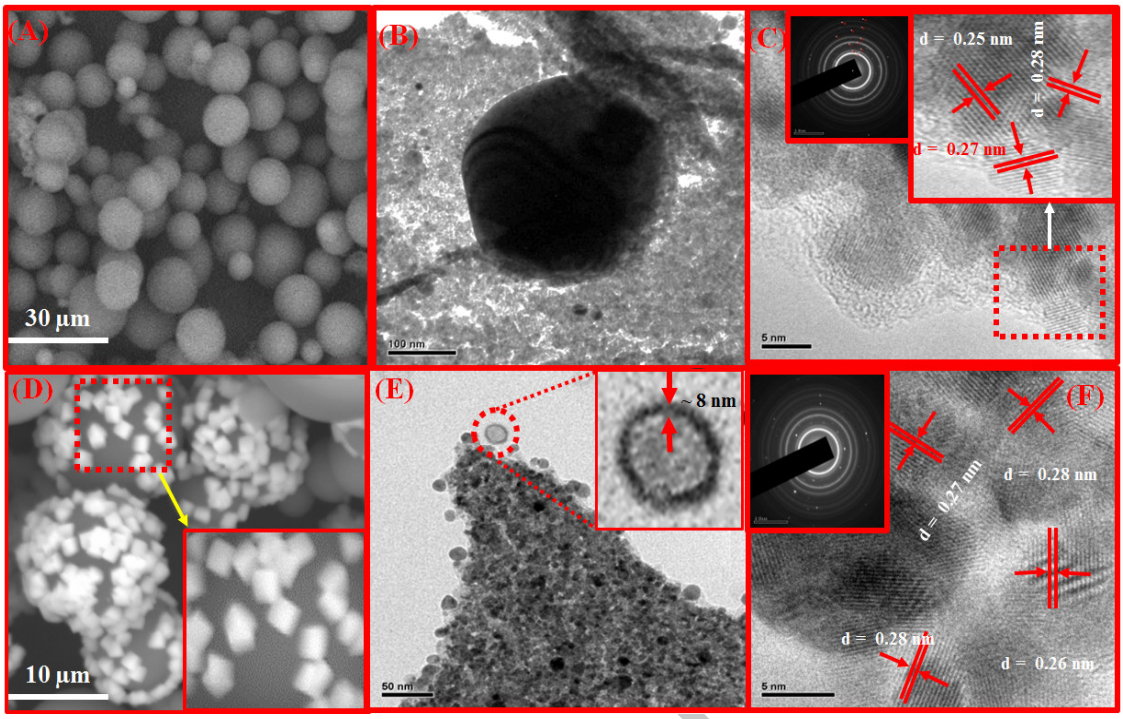

Fig.5. SEM, TEM & HRTEM images of (A-C) SiO_2 and (D-F) SiO_2@$SrTiO_3$:Eu^{3+} (1 mol %): Li^+ (1 wt %) NP.

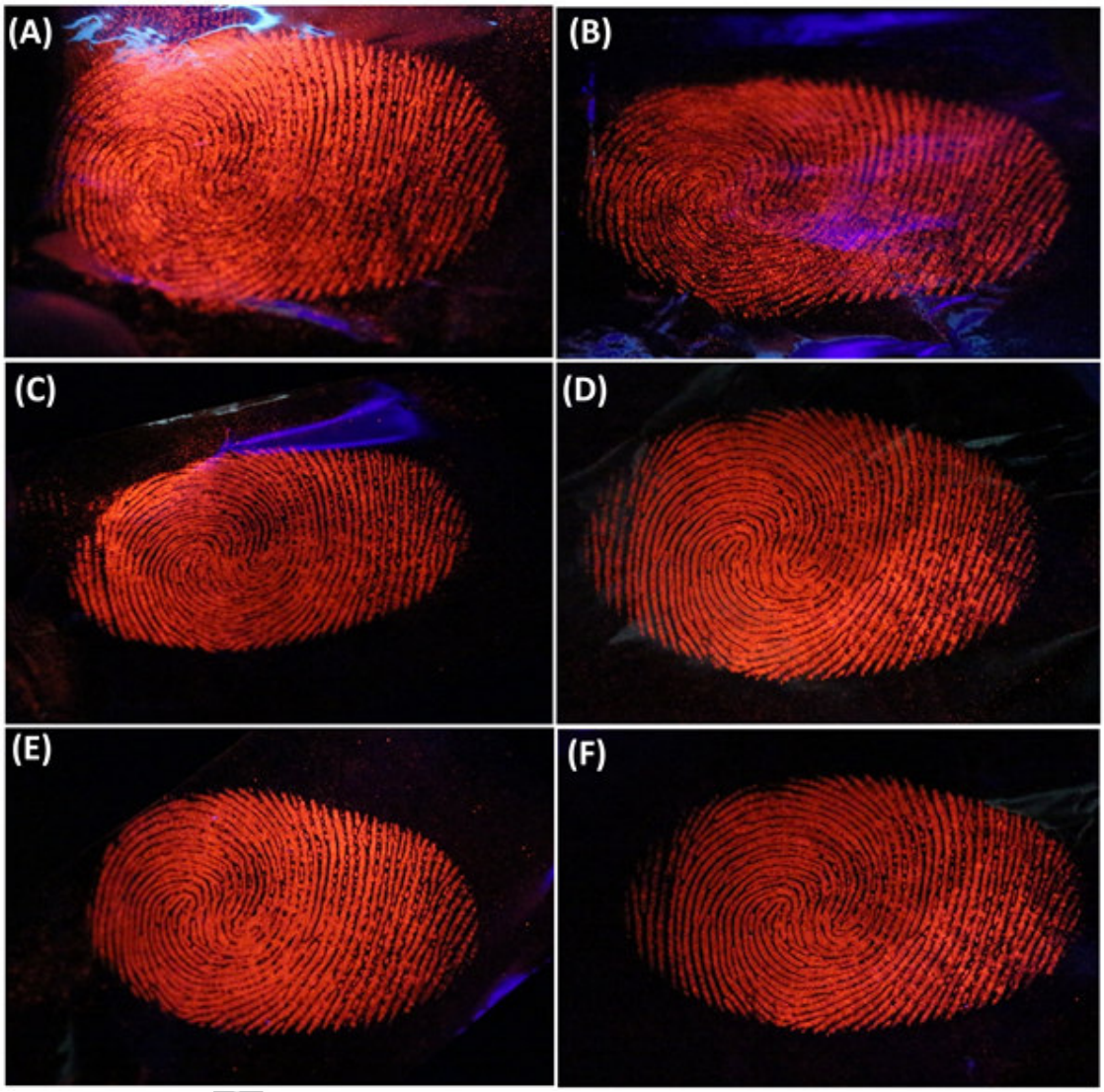

Fig.6. LFPs visualized by staining $SrTiO_3:Eu^{3+}$: (1 mol %): Li^+ (1 wt %) NPs coated on the surface of SiO_2 core shells with different coat (1-6).

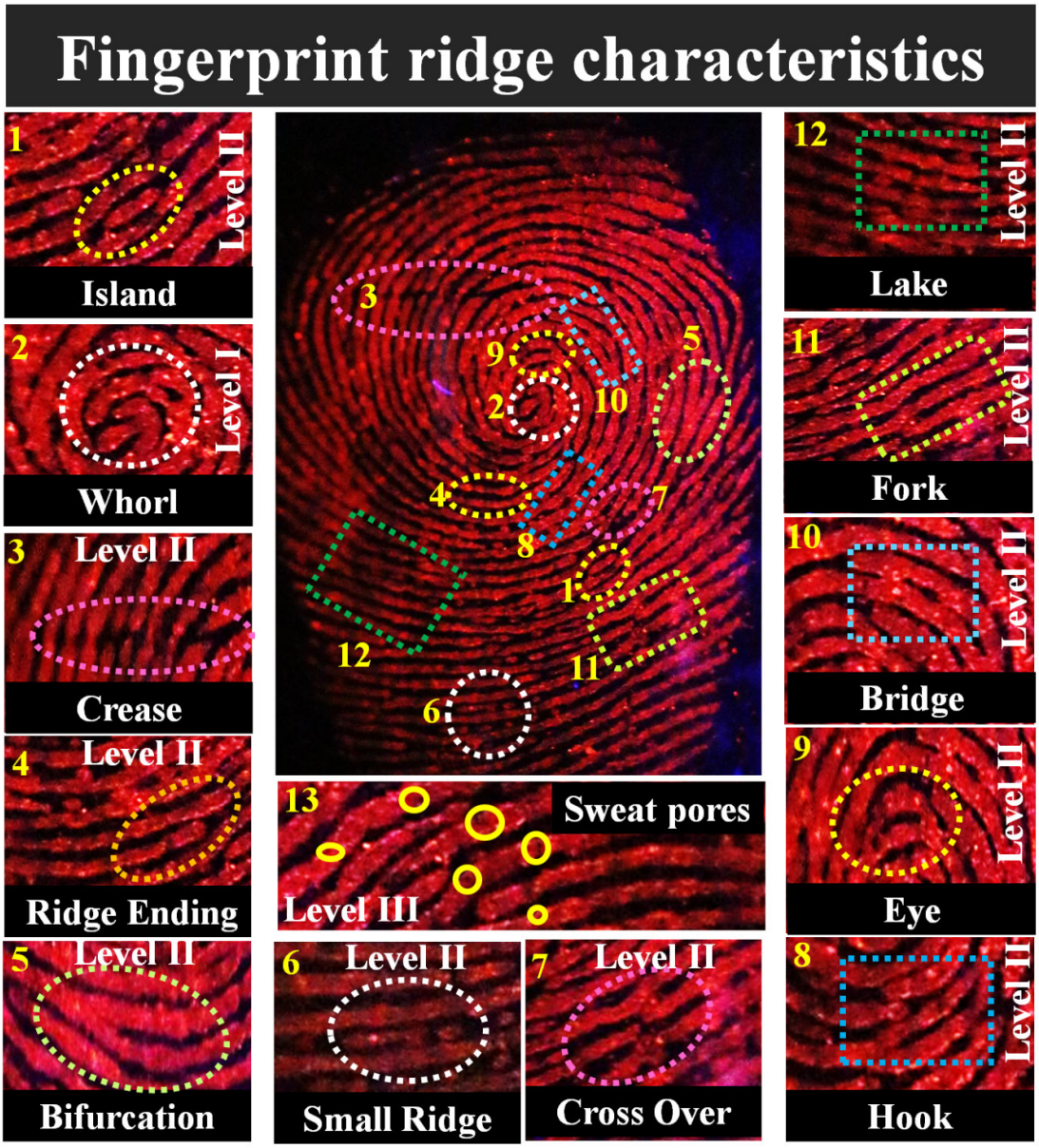

Fig.7. Various ridge details of LFPs visualized using optimized SiO_2@$SrTiO_3$:Eu^{3+} (1 mol %):Li^+ (1 wt %) NPs on glass surface under UV 254 nm.

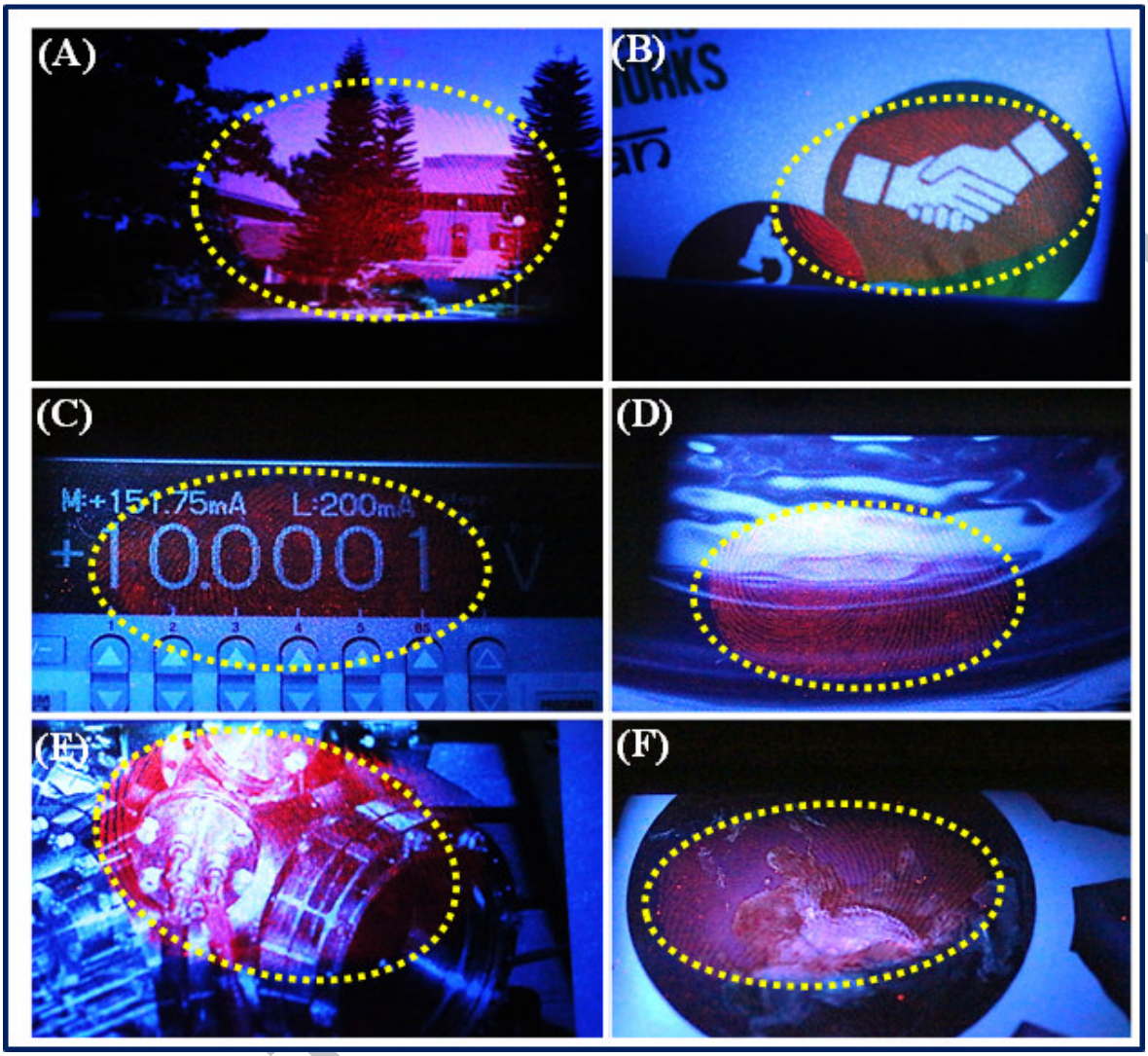

Fig.8. LFPs visualized by staining SiO_2@$SrTiO_3$:Eu^{3+} (1 mol %): Li^+ (1wt %) NP by powder dusting method on porous surfaces.

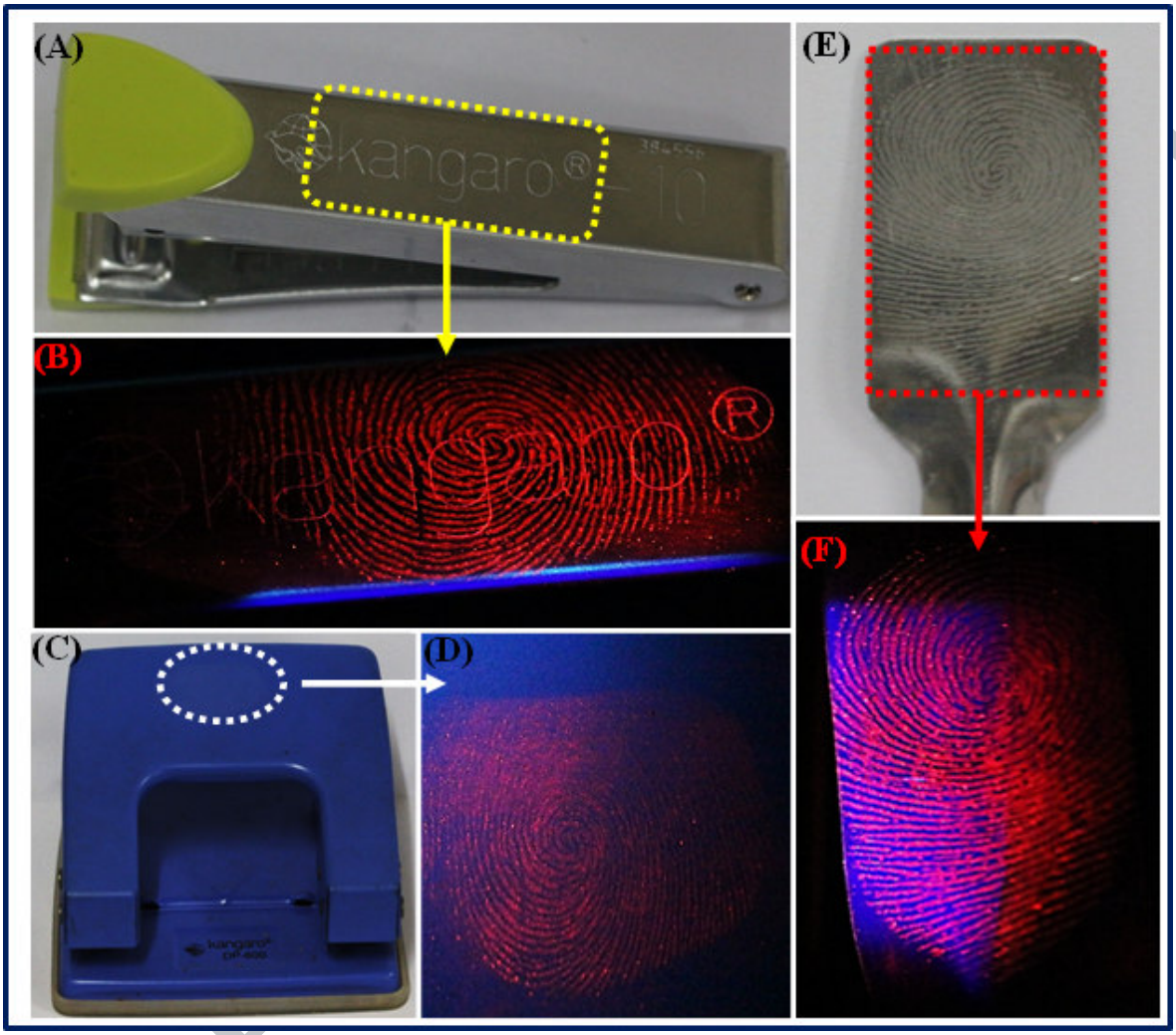

Fig.9. LFPs visualized by staining SiO_2@$SrTiO_3$:Eu^{3+} (1 mol %): Li^+ (1wt %) NP on various non-porous surfaces.

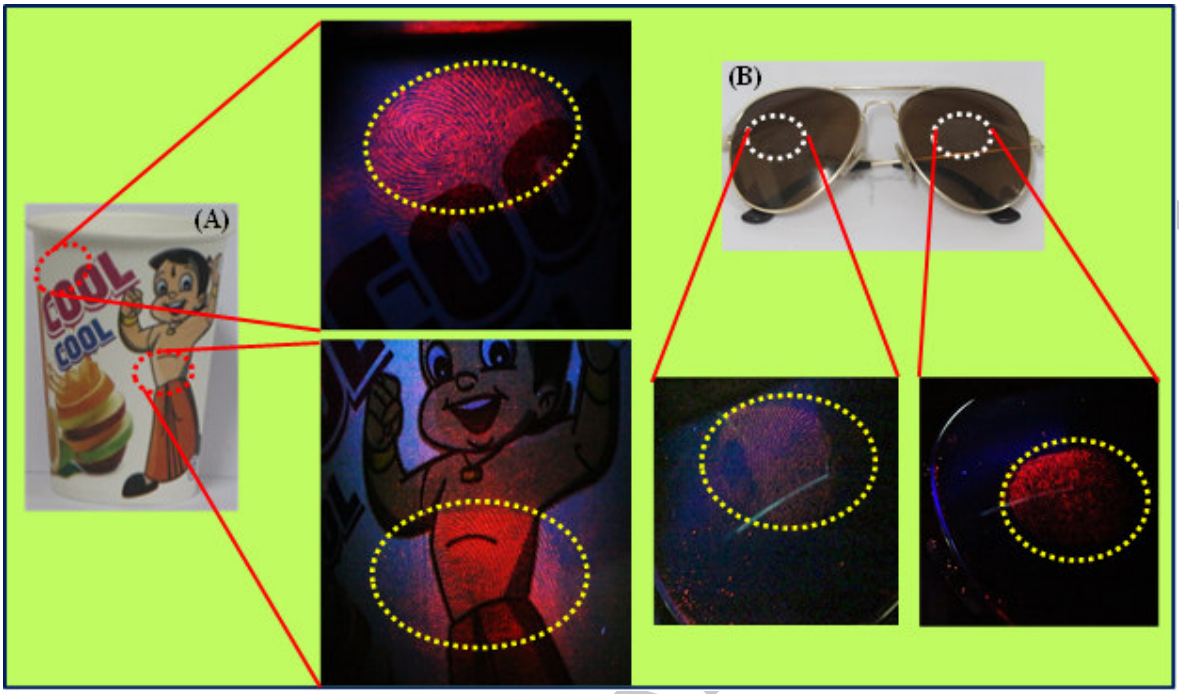

Fig.10. LFPs visualized by powder dusting method by staining SiO_2@$SrTiO_3$:Eu^{3+} (1 mol %):Li^+ (1wt %) NPs on the surface (A) paper cup and (B) goggle under 254 nm.

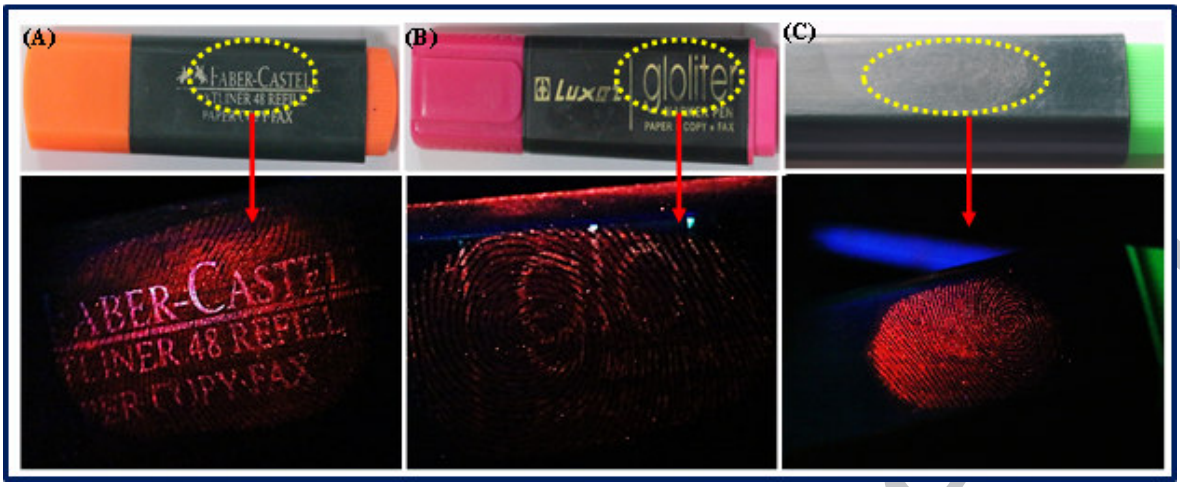

Fig.11. LFPs visualized by staining SiO_2@$SrTiO_3$:Eu^{3+} (1 mol %):Li^+ (1wt %) NP on the surface of various highlighters under 254 nm.

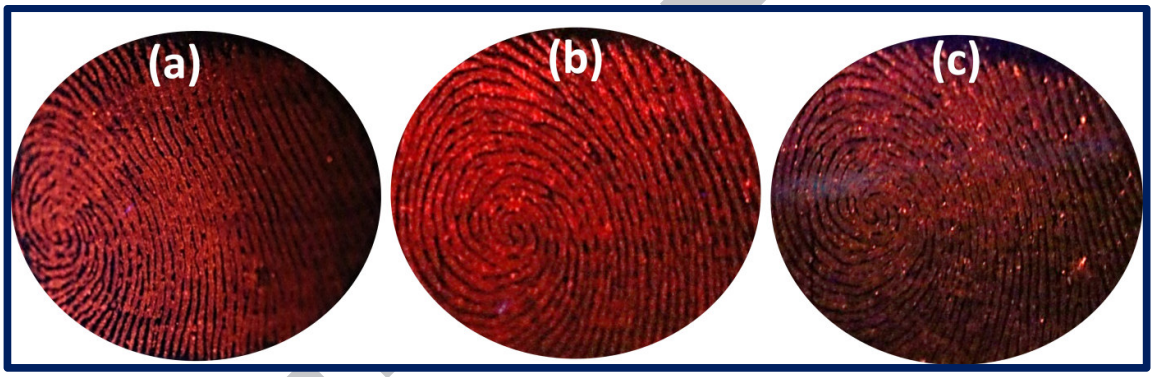

Fig.12. LFPs aged on the surface of aluminum foil for various periods of time, stained by SiO_2@$SrTiO_3$:Eu^{3+} (1 mol %): Li^+ (1 wt %) NP under UV 254 nm: (a) 1 day, (b) 1 week, (c) 3 weeks.

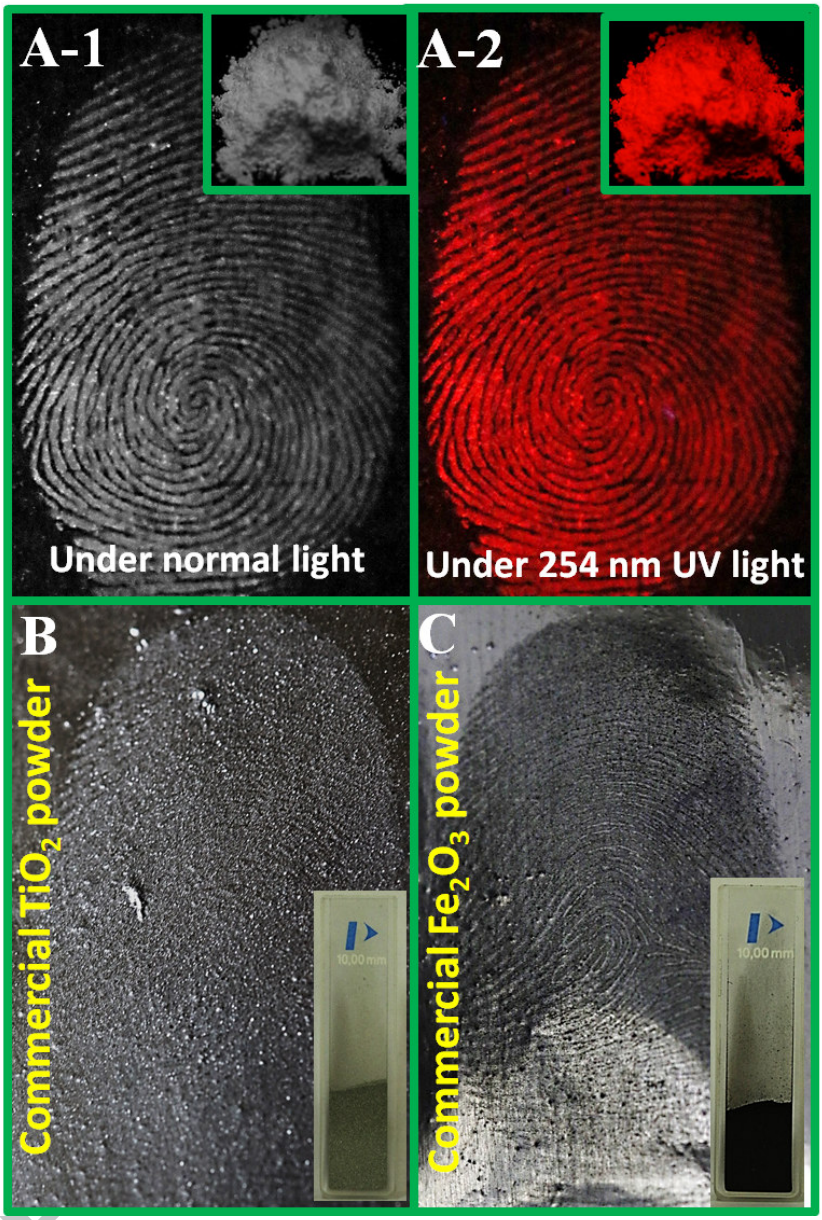

Fig.13. LFPs on the surface of glass stained by (A-1 & A-2) SiO_2@$SrTiO_3$:Eu^{3+} (1 mol %):Li^+ (1 wt %) NP under normal and UV 254 nm light, (B) TiO_2 powder and (C) magnetic iron oxide powder under normal light.

Fig.14. LFPs stained by SiO_2@$SrTiO_3$:Eu^{3+} (1 mol %):Li^{+} (1 wt %) on (A & B) currency paper, (C & D) credit card and (E & F) coin under 254 nm.

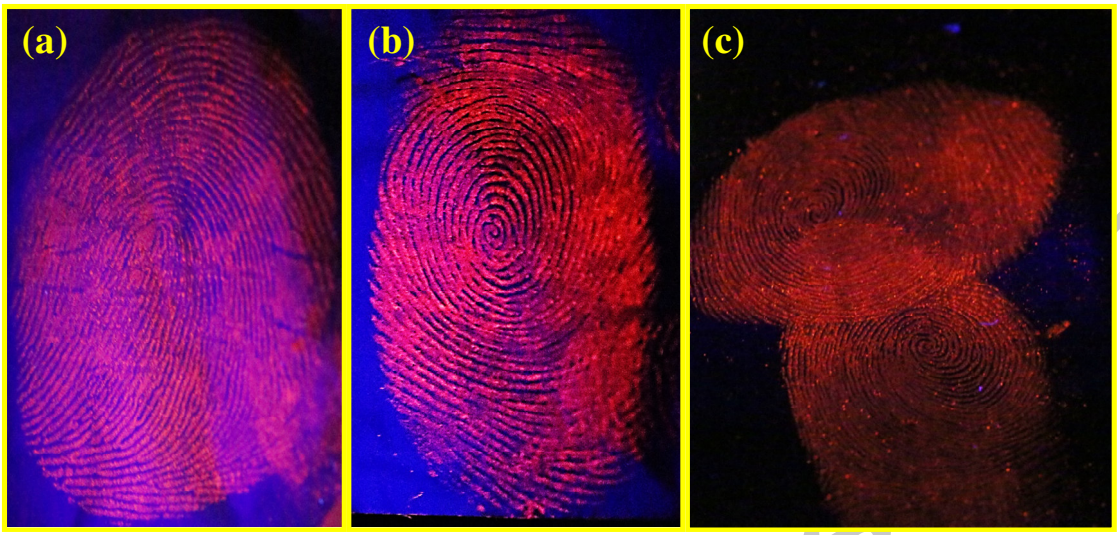

Fig.15. LFPs visualized by optimized SiO_2@$SrTiO_3$:Eu^{3+} (1 mol %):Li^+ (1 wt %) NP stored for ~ 2 months at room temperature.

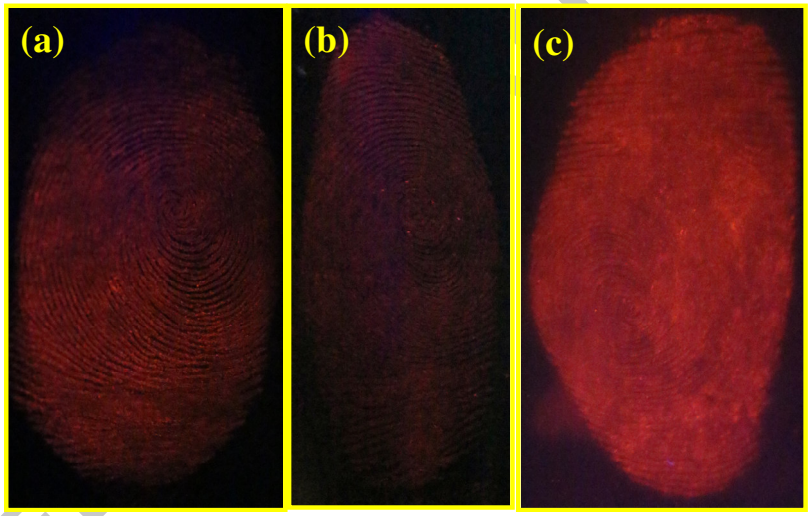

Fig.16. LFPs visualized by optimized SiO_2@$SrTiO_3$:Eu^{3+} (1 mol %): Li^+ (1 wt %) NP by maintain different temperature (a) 27 °C, (b) 35 °C and 38 °C.

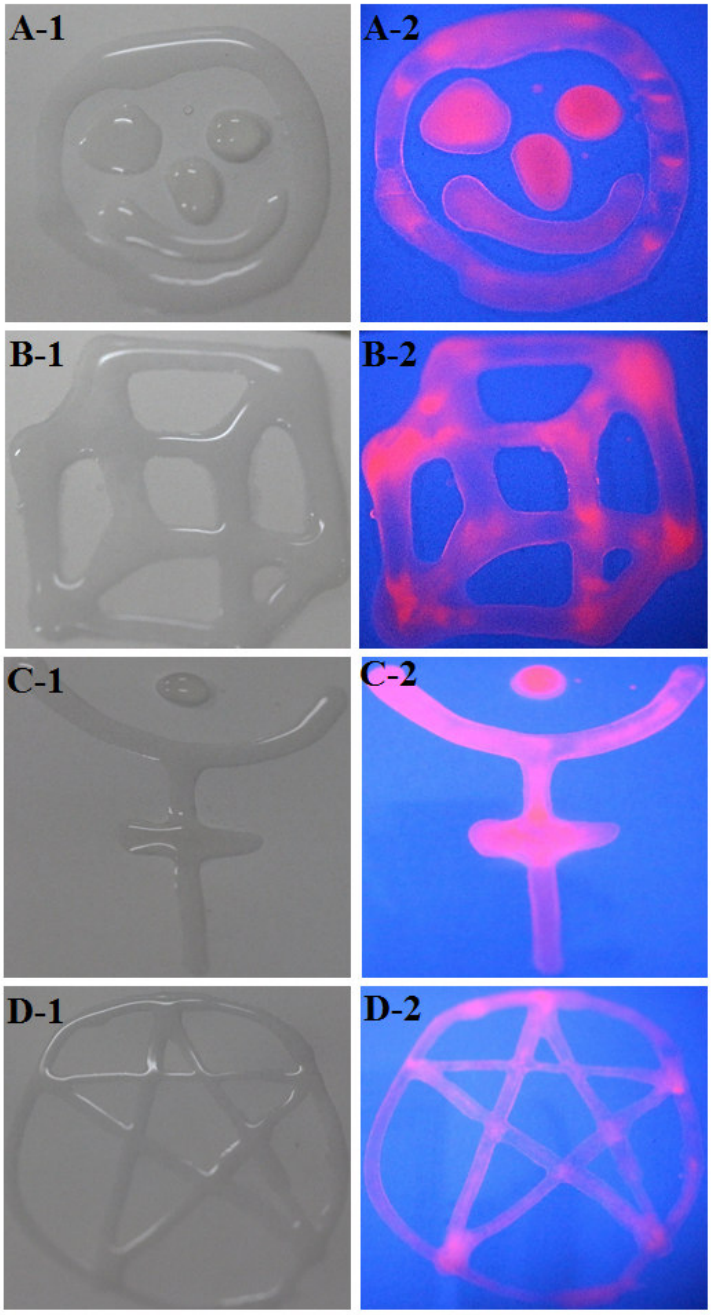

Fig.17. Anti-counterfeiting labels painted with SiO_2@$SrTiO_3$:Eu^{3+} (1 mol %): Li^+ (1 wt %) NP ink under (A1–D1) visible light and (A2–D2) UV 254 nm light.

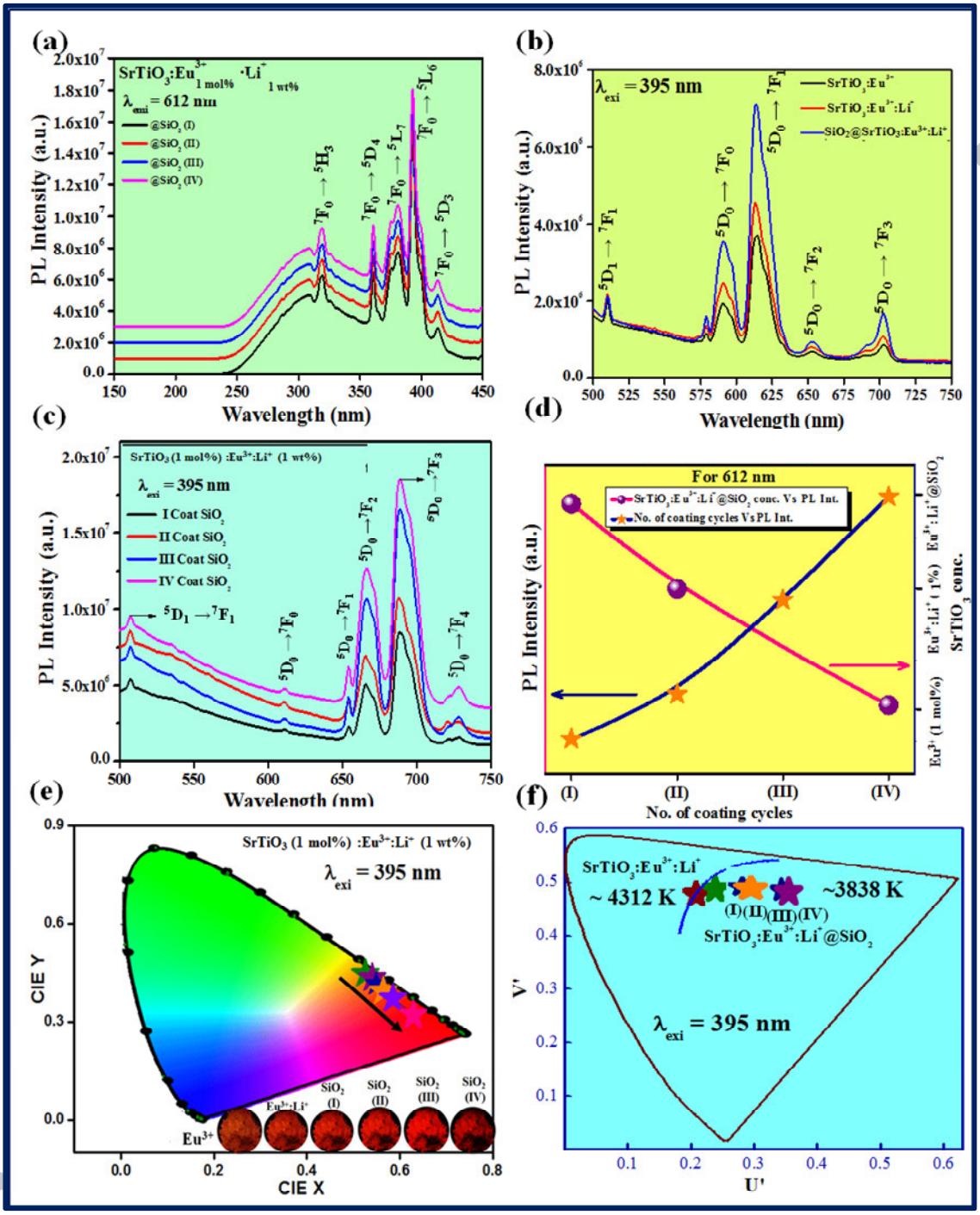

Fig.18 (a) PL excitation spectrum, (b) emission spectra under 395 nm excitation, (c) emission spectra of $SrTiO_3$:Eu^{3+}: (1 mol %): Li^+ (1 wt %) NPs coated on the surface of SiO_2 core shells with different coat (1-6), (d) variation of PL intensity with respective to $SrTiO_3$ concentration & number of coating cycles, (e) CIE and (f) CCT diagram of SiO_2@$SrTiO_3$:Eu^{3+} (1 mol %):Li^+ (1 wt %) with different coat.

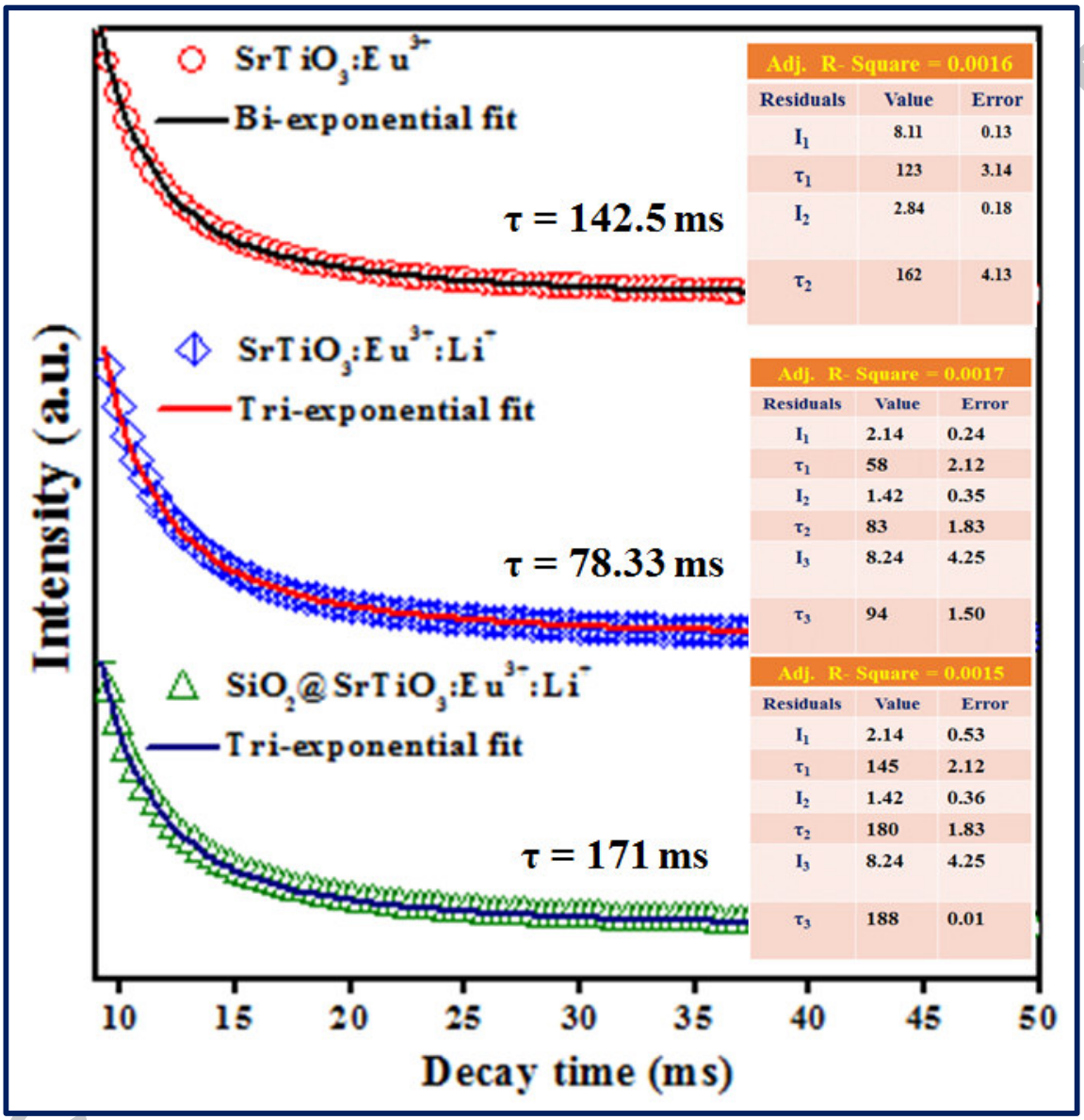

Fig.19. Decay curves of (1) $SrTiO_3:Eu^{3+}$ (2) $SrTiO_3:Eu^{3+}$, Li (1 wt %) (3) SiO_2@ $SrTiO_3:Eu^{3+}$, Li (1 wt %) NPs.

Table 1: Hazards of various reagents used for LFPs detection.

Sl.No	Chemicals	Hazards
1	Ninhydrin solution	Flammable. Harmful vapours. Skin and eye irritant.
2	DFO (1,8-diazafluoren-9-one) solution	Flammable. If inhaled it may be quit dangerous. May be absorbed through the skin. Respiratory and digestive region irritant. May cause skin and eye irritation.
3	Silver nitrate solution	Oxidizer. May be harmful if inhaled. Respiratory and digestive tract irritant. May cause skin and eye burns, argyria, a blue-gray discoloration of the skin, eyes, and mucous membranes.
4	Cyano acrylate glue	Respiratory tract, eye and skin irritant. Bonds skin rapidly and strongly. May cause skin burns.
5	Iodine crystals	Oxidizer. May be harmful if inhaled, ingested, or contacted by skin or eyes. Respiratory irritation. May be corrosive to skin and eyes.
6	Gentian violet solution	May be absorbed through the skin. Respiratory, digestive, skin and eye area will get aggravation.

Table 2: Indicates the stability and aging of prepared NPs with the commercial dusting powders.

Sl. No.	Powder type	Glass surface	White Ceramic	Black marble	Aluminium foil	Coin	References
1	TiO_2 powder	A-grade	C-grade	A-grade	C-grade	C-grade	[19]
2	Iodine Vapour	A-grade	A-grade	C-grade	C-grade	C-grade	[20]
3	Cyanoacrylate glue vapour	A-grade	C-grade	A-grade	C-grade	C-grade	[21]
4	Fluorescence starch powder	A-grade	A-grade	A-grade	A-grade	B-grade	[22]
5	SiO_2@$SrTiO_3$:Eu^{3+}:Li core-shell nanopowder	A-grade	A-grade	A-grade	A-grade	B-grade	Present work

Table 3: Judd-Ofelt intensity parameters (Ω_2 & Ω_4), radiative transition probability (A_T), calculated radiative (τ_{rad}) lifetime, branching ratio (β_R), asymmetric ratio (A_{21}) and stimulated emission cross section (σ_e) of prepared samples (λ_{exi} = 395 nm).

Compound	**J – O intensity parameters ($\times 10^{-20}$ cm^2)**		**A_T (s^{-1})**	**τ_{rad} (ms)**	**β_R**	**A_{21}**	**σ_e ($\times 10^{-30}$ cm^2)**
	Ω_2	**Ω_4**					
$SrTiO_3:Eu^{3+}$	2.78	0.84	68.12	16.21	0.99	1.94	0.18
$SrTiO_3:Eu^{3+}:Li^+$	2.42	0.87	61.23	18.23	0.98	1.68	0.16
$SiO_2@SrTiO_3:Eu^{3+}:Li^+$	2.33	0.88	60.18	19.22	0.97	1.65	0.15

Table 4: CIE and CCT values of prepared NPs.

Compound	CIE				CCT (K)
	x	y	U^1	V^1	
$SrTiO_3:Eu^{3+}$ (1 mol %)	0.5253	0.4466	0.3183	0.4872	4352
$SrTiO_3:Eu^{3+}$ (1 mol %): Li^+ (1 wt %)	0.5404	0.4334	0.3284	0.4976	4321
SiO_2@$SrTiO_3:Eu^{3+}:Li^+$ (I coat)	0.5491	0.4150	0.3184	0.4877	3921
SiO_2@$SrTiO_3:Eu^{3+}:Li^+$ (II coat)	0.5644	0.3944	0.3286	0.4975	3788
SiO_2@$SrTiO_3:Eu^{3+}:Li^+$ (III coat)	0.5849	0.3711	0.2085	0.4773	3815
SiO_2@$SrTiO_3:Eu^{3+}:Li^+$ (IV coat)	0.5812	0.3723	0.2081	0.4754	3811

Research highlights

- Core–shell SiO_2@$SrTiO_3$:Eu^{3+}:Li^+ nanopowders were prepared by easy way.
- Increased coating of shell tuned the emission from orange-red to the deep red.
- The PL intensity was increased two folds in coated phosphors than non-coated.
- Samples were efficient to use in Forensic and anti-counterfeiting applications.

Graphical Abstract